Inter-El Niño variability in CMIP5 models: Model deficiencies and future changes

Kyung-Sook Yun[1], Sang-Wook Yeh[3], and Kyung-Ja Ha[1, 2*]

[1]Research Center for Climate Sciences, Pusan National University, Busan 46241, Korea

[2]Department of Atmospheric Sciences, College of Natural Science, Pusan National University, Busan, Korea

[3]Department of Marine Sciences and Convergent Technology, Hanyang University, ERICA, Korea

[*]Corresponding author: Kyung-Ja Ha (kjha@pusan.ac.kr)

This article has been accepted for publication and undergone full peer review but has not been through the copyediting, typesetting, pagination and proofreading process which may lead to differences between this version and the Version of Record. Please cite this article as doi: 10.1002/2016JD024964

Abstract

Inter-El Niño variability, which represents the diversity in spatiotemporal evolution among El Niño events, has been identified using the first two leading modes of sea surface temperature anomalies along the equator. The first mode represents the transition from El Niño into La Niña and the second mode reveals El Niño's persistence through the following spring. Here, we examine the ability of models to capture inter-El Niño variability and predict future changes due to global warming using historical and Representative Concentration Pathway 8.5 simulations of phase 5 of the Coupled Model Intercomparison Project (CMIP5). Most CMIP5 models realistically reproduce the first mode, but three-fifths of the models fail to capture the second mode, with considerable inter-model diversity. The ten best models are therefore selected according to a measurement of pattern correlation coefficients and normalized root mean square with respect to reproduction of the second mode. The results aggregated from the best models indicate that the first "transition" mode will remain unchanged from the present climate to the future climate; in contrast, the second "persistence" mode changes stochastically across the CMIP5 models. Consequently, we conclude that El Niño's transition into La Niña is the most dominant characteristic of simulated inter-El Niño variability and will remain unswayed under global warming conditions. Model deficiency in simulating El Niño's persistence is a key source of uncertainty in modeling inter-El Niño variability, resulting in difficulty predicting how certain characteristics of El Niño events may change with global warming.

1. Introduction

El Niño-Southern Oscillation (ENSO) is one of the most important interannual fluctuations of an atmosphere-ocean coupled system. Its worldwide implications have prompted efforts to expand our understanding of ENSO dynamics and characteristics [e.g., *Jin*, 1997, *McPhaden et al.*, 2006; *Kug et al.*, 2009; *Yu et al.*, 2012]. In particular, recent studies have shown a renewed interest in differences among ENSO events, which are called inter-ENSO variability or ENSO diversity [*Lopez and Kirtman*, 2013; *Lee et al.*, 2014; *Yeh et al.*, 2014; *Capotondi et al.*, 2015]. Note that considerable differences are not only revealed in the maximum location and strength of ENSO sea surface temperature anomalies (SSTA) but also in their temporal evolution [*Ha et al.*, 2012]. A better understanding of inter-ENSO variability with respect to spatiotemporal evolution is therefore a prerequisite for the study of ENSO-induced teleconnections and impacts [*Capotondi et al.*, 2015].

In light of El Niño's event-to-event variation, it has been increasingly recognized that there are two different spatial types of El Niño events. One is the eastern-Pacific (EP) El Niño that is centered over the eastern Pacific Niño 3 region; the other is the central-Pacific (CP) El Niño that occurs over the Niño 4 region [*Kao and Yu*, 2009; *Kug et al.*, 2009; *Yeh et al.*, 2009]. Relevant dynamics exhibit significant differences between the EP- and CP- El Niño. For example, the thermocline feedback is more effective in driving the EP- El Niño,

whereas zonal advection feedback has a greater contribution to inducing the CP- El Niño [e.g., *Kug et al.*, 2009]. Variation in the temporal evolution of El Niño has also been explored, in particular the onset and termination of El Niño, with a focus on El Niño's transition to La Niña. For instance, variability of anomalous wind forcing in the western tropical Pacific and North Pacific subtropical high, which is affected by abnormal warming in the Indian Ocean and local air-sea interaction, play a key role in modulating the rapid transition to La Niña via the thermocline adjustment and equatorial Kelvin wave responses [*Wang et al.*, 1999; *Kim and Lau*, 2001; *Kug and Kang*, 2006; *Yun et al.*, 2015; *Chen et al.*, 2016].

Previous studies have also shown the divergent impacts of greenhouse warming on ENSO [*Yeh et al.*, 2009; *Bellenger et al.*, 2014; *Kim et al.*, 2014; *Cai et al.*, 2014; 2015; *Chen et al.*, 2015]. Climate models project no robust changes in ENSO amplitude [*Collins et al.*, 2010; *Stevenson*, 2012; *Power et al.*, 2013]. *Chen et al.* [2015] demonstrated that the projected diversity in ENSO amplitude originates from changes in ENSO meridional width, by modulating thermocline and zonal advection feedbacks. The occurrence of CP- El Niño events relative to EP- El Niño is expected to increase in the model simulations under global warming conditions [*Yeh et al.*, 2009; *Kim and Yu*, 2012; *Taschetto et al.*, 2014]. These changes were primarily attributable to weakened equatorial upwelling and thermocline feedback in future scenarios. The frequency of extreme El Niño events is also projected to increase due to greenhouse warming, as a consequence of mean state changes [*Cai et al.*,

2014]. Several studies have drawn attention to changes in the temporal evolution of ENSO but no significant changes emerge across all models [*Taschetto et al.*, 2014; *Chen et al.*, 2016]. This indicates that ENSO diversity might increase due to greenhouse warming.

Recently, an observational study by *Lee et al.* [2014] attempted to show the spatiotemporal SST evolution of inter-El Niño variability using empirical orthogonal function (EOF) analysis in a time-latitude domain averaged over the equator [5°S-5°N] (see Fig. 1). It was noted that the first mode represents the extent to which warm SSTAs in the EP persist into the boreal spring after the El Niño peak (i.e., persistent mode), whereas the second mode reveals the transition and resurgence of El Niño in the decaying year (i.e., transition mode). This study raises an important question regarding how well the current climate models capture the two major observed modes of El Niño events. The major objective of the present study is therefore (1) to examine the models' capacity in capturing the spatiotemporal evolution of inter-El Niño variability and (2) to explore how inter-El Niño variability will change in the future, using historical and representative concentration pathway 8.5 (RCP8.5) simulations of phase 5 of the Coupled Model Inter-comparison Project (CMIP5). La Niña events show subtler inter-event variation of spatial patterns [*Capotondi et al.*, 2015]. For this reason, we focus only on the inter-El Niño variability. Here, we use 40 available climate models and provide a comprehensive overview of their performance in reproducing the inter-El Niño variability.

The remainder of this paper is organized as follows. Sections 2 presents the CMIP5 model data and methodology for assessing the inter-El Niño variability. Section 3 describes the models' performance in reproducing the inter-El Niño variability in a historical simulation. Section 4 depicts possible future changes to inter-El Niño variability. Section 5 discusses and summarizes the results.

2. Datasets and methods

2.1 CMIP5 model data

A total of 40 coupled general circulation models (CGCMs) that participated in the CMIP5 were used [*Taylor et al.*, 2012]. A historical simulation (i.e. the twentieth-century experiment) for the period of 1900-2005 was applied to examine the models' abilities to reproduce the observed spatiotemporal evolution of inter-El Niño variability. The historical run imposed changing conditions that were consistent with observations, including natural and anthropogenic forcings. For future climate projections, an RCP8.5 run, in which radiative forcing continuously rises toward 8.5 W/m^2 in 2100, was analyzed during the period from 2006 to 2099. To reduce uncertainties in models, we used members of ensemble as many as possible in each model experiment. Details of the 40 CMIP5 models are listed in Table 1.

To assess model performance with respect to observation data (OBS), this study used SST data from 1900 to 2014 obtained from Met Office Hadley Centre Sea Ice and Sea

Surface Temperature version 1.1 (HadISST1.1) [*Rayner et al.*, 2003]. To ensure fair comparisons, all data were interpolated to a common grid of 2.5°× 2.5°. Before applying all analyses, we performed variance correction of modeled SSTA for two major reasons. The first is attributable to considerable inter-model diversity in ENSO amplitude, as reported in many previous studies [e.g, *Bellenger et al.*, 2014; *Kim et al.*, 2014; *Cai et al.*, 2015]. The large inter-model spread in ENSO amplitude can lead to misinterpretation of the results based on a multi-model average. The second reason for variance correction was to focus our purpose on examining the phase transition and persistence of inter-El Niño variability, not the amplitude. At each grid point, we first computed a standard deviation of modeled SSTA for each model ($M\sigma_{s,n}$) and a standard deviation of observed SSTA ($O\sigma_s$). The SSTA variability of each model was then normalized to the observed variability as follows.

$$Cor\_SST_{s,t,n} = SST_{s,t,n} / M\sigma_{s,n} \times O\sigma_s \quad (1)$$

where $SST_{s,t,n}$ indicates the modeled SSTA for each grid point (s), time (t), and model (n).

2.2 Spatiotemporal evolution of inter-El Niño variability

To define El Niño years, the monthly Niño3.4 index [5°S-5°N, 170°W-120°W] was used. Monthly SSTA was first obtained by removing the seasonal cycle and linear trends from the OBS and from each model. Note that the modeled Niño3.4 SSTA shows a linear increasing

trend in the historical and RCP8.5 runs (figure not shown). The de-trending permits unbiased selection between warm and cold events of ENSO through the entire period, excluding global warming effect. The El Niño years were then identified based on the following threshold: the 3-month running mean of Niño3.4 SSTAs exceed 0.5°C for at least five consecutive months, following the definition used at the National Centers for Environmental Prediction (NCEP). Finally, 1101 El Niño years, a sum across all 40 models, were identified during the period of 1900-2005 in the historical runs, whereas 994 El Niño years were selected during the period of 2006-2099 in the RCP8.5 runs. The El Niño event numbers from each model are shown in Table 1. The mean number of events in the historical runs is 27.5, which is compared to 32 El Niño years observed during the period of 1900-2014.

The present study used an objective methodology to identify two major modes of inter-El Niño variability based on the longitude-time maps of equatorial SSTAs, as introduced by *Lee et al.* [2014]. According to this methodology, we conducted an empirical orthogonal function (EOF) analysis for the longitude-time domains of SSTA averaged over the equator [5°S-5°N] for each individual event. The reconstructed spatiotemporal EOF domain consisted of longitude (x-axis) ranging from 120°E to 90°W and monthly variance (y-axis) spanning from January of the developing year to December of the decaying year. The inter-event variability is given by the principal component (PC) time series. This provides an efficient metric for depicting the continuum of inter-El Niño evolution. The two leading EOF modes in

the OBS explain about 54% of the total variance. The two leading modes (see Figs. 1a and b) are essentially consistent with the results from *Lee et al.* [2014] but the persistence (transition) mode is seen as EOF2 (EOF1). This is caused by longer time period and different SST dataset used (figure not shown).

3. Inter-El Niño variability in CMIP5

We first examine the composite mean (CM) evolution of El Niño SSTA along the equator in the historical run (1900-2005), as a function of longitude and calendar month (Fig. 2). Here, the CM indicates the mean pattern of SSTA averaged for El Niño years of each model. The SSTA variability of each model is normalized to the observed counterpart before analyzing the CM (see Section 2.1). Compared to the observed CM (see Fig. 1c), the modeled CMs reproduce El Niño's maximum and seasonal evolution reasonably well with high pattern correlation coefficients (PCCs) above 0.7, as shown in the upper right corner of each panel in Fig. 2. Except for IPSL-CM5A-LR, El Niño in most models develops during the boreal summer and decays after the winter peak (i.e., November-December-January). Figure 3a summarizes the model performance for simulating the CM based on the normalized root mean square error (NRMSE) and PCC between the OBS and the individual CMIP5 models. Here, NRMSE indicates domain-averaged RMSE normalized to the observed standard deviation. Most models have a high fidelity in capturing the El Niño CM, as demonstrated by

a strong linear relationship between RMSE and PCC (correlation coefficient r ~ -0.88). Similarly good performance is also seen in the temporal correlation coefficients (TCCs) between observed and simulated Niño 3 and Niño 4 SSTA CMs (Fig. 3b). Of particular note is that the TCC of Niño 3 is uncorrelated with that of Niño 4 (r ~ 0.26). The CMIP5 discrepancies in El Niño's seasonality between the EP and CP also agree closely with the result in *Taschetto et al.* [2014]. Contrary to OBS and other models, several models (e.g., FIO-ESM and GFDL_ESM2M) show the warmest anomalies developing first in the west and growing to the east. The IPSL-CM5A-LF and MIROC5 are the poorest performing models that exhibit El Niño's summer peak and longer-lasting warming, respectively. The modeled strength of SSTA also reveals large variation between CMIP5 models: CESM1-CAM5 is strongest, while inmcm4 is weakest.

The observed EOF1 mode depicts whether El Niño has transitioned into La Niña (Fig. 1a), whereas the EOF2 mode describes whether a strong El Niño event will persist into the boreal spring (March-April-May) of the decaying year (Fig. 1b). The CMIP5 historical simulations capture the first two observed leading modes, as shown in the spatiotemporal pattern of the first two modeled EOF modes (Figs. 4 and 5). The most important feature of the modeled inter-El Niño variability is the transition mode (i.e., EOF1; Fig. 4). Compared to the OBS, most CMIP5 models capture the transition mode reasonably well. Particularly, the bcc-csm1-1-m and NorESM1-ME most realistically reproduce the transition from warm to

cold phases. In several models, the maximum warm SST anomalies appear during the MAM(0) of the developing year (e.g., CSIRO-Mk3-6-0), and the minimum cold SST anomalies emerge in the fall (September-October-November(+1)) of the decaying year (e.g., GISS-E2-H). These peak positions are quiet different from the observed maximum during the SON(0) of the developing year and observed minimum during the winter (NDJ(+1)) of the decaying year, which indicates a marked bias in these models.

On the other hand, the CMIP5 models have large inter-model diversity in simulating the persistence mode (EOF2), as shown in Fig. 5. The great inter-model diversity may be caused by different physics, dynamics, initial conditions, and resolution in CMIP5 models. It should be noted that the model spread in CMIP5 projection is dependent on internal climate variability and model error that are difficult to disentangle in CMIP5 model ensemble. Therefore, it would be useful to analyze a large ensemble simulation of climate model [e.g., *Kay et al.*, 2015]. Generally, CESM1 models (i.e., CESM1-CAM5, CESM1-CAM5.1-FV2, CESM1-WACCM) effectively reproduce the feature revealing springtime persistence. Three-fifths of the 40 CMIP5 models fail to reproduce the EOF2 mode. For example, CSIRO-Mk3-6-0, IPSL-CM5A-LR, IPSL-CM5A-MR, and MPI-ESM-MR are the poorest performing models that show the warming maximum in EOF2 during the FMA(0) or SON(+1) season.

The percentage of modeled variance explained by EOF shows considerable inter-model spread, ranging from 27.9 to 56.4% for EOF1 and from 12.7 to 30.8% for EOF2 (Fig. 6).

Note that the percentage of variance by EOF1 tends to be overestimated by most CMIP5 models; in contrast, the modeled variances of EOF2 are equivalent to the OBS. The models' performance in reproducing the two leading modes is further explored by comparing the NRMSEs and PCCs of EOF1 and EOF2 between OBS and the models (Fig. 7a). As mentioned earlier, most CMIP5 models reproduce the spatiotemporal pattern of EOF1 well, ranging from 0.71 to 0.95 PCC and from 0.31 to 1.0 NRMSE. The two poorest performing models (IPSL-CM5A-MR and CSIRO-Mk3-6-0) still exhibit significant PCCs that exceed 0.6. Interestingly, the models' skill in capturing EOF1 tends to be related to their ability to reproducing EOF2 ($r \sim 0.32$), implying that internal model dynamics affect their ability to capture inter-ENSO variability.

Compared to EOF1, there is considerable inter-model diversity in EOF2 performance, which is a relatively poor. The PCCs and RMSEs have divergent ranges of -0.18 to 0.89 and 0.47 to 1.7, respectively. Consequently, the inability of climate models to realistically simulate the EOF2 mode is an important source of uncertainties and model deficiency with respect to inter-El Niño variability. The ten best models were chosen for further analysis, based on a PCC performance greater than 0.75 and a NRMSE exceeding 0.8 for EOF2; CESM1-CAM5, CESM1-CAM5.1-FV2, CESM1-WACCM, CMCC-CM, CMCC-CMS, FGOALS-g2, GFDL-ESM2M, HadGEM2-CC, MIROC5, and NorESM1-ME (see Fig. 7b).

4. Future change due to global warming

How ENSO diversity will change in a warming climate is currently one of the most significant issues in climate change science [*Capotondi et al.*, 2015; *Cai et al.*, 2015]. In this section, we examine the projected future changes of inter-ENSO variability in the historical runs due to global warming using the RCP8.5 simulations. Although three-fifths of the models fail to reproduce the leading mode of inter-ENSO variability, the ten best models produce reasonable leading modes of El Niño transition and persistence. Hereafter, most analyses show results from the ten best multi-model mean (i.e., B10MMM). All analyses are first performed in each model and the B10MMM is then calculated by averaging the results derived from the ten best models.

Before analyzing the change in leading modes, we investigate the change in the El Niño CM using the B10MMM results. Figure 8 displays the temporal evolution of CM for Niño 3.4 SST anomalies in the historical and RCP8.5 simulations, respectively, for each model. The SST evolution, which varies considerably across the models, shows no significant change between the present and future climates. Under the future climate scenario, a slight change is projected by weaker (or earlier) maximum and a more rapid decay of El Niño evolution during the MAM(+1).

We next explore changes in inter-El Niño leading modes. Although several biases still appear in the B10MMM, the B10MMM realistically simulates the two observed leading

modes during El Niño events (Fig. 9). Compared to the OBS, the modeled probability that phases of PC1 and PC2 occur is overestimated in the phases of positive PC1 and PC2 (+8.6%) and negative PC1 and PC2 (+1.4%), while the probability is underestimated in the phases of positive PC1 and negative PC2 (-3.9%) and negative PC1 and positive PC2 (-5.8%). Only two small changes are revealed between the present and future climates. First, the occurrence of a negative PC1 and positive PC2 phase tends to decrease, but the probability of other phases increases. Second, the CP warming in EOF2 is likely to decay earlier in the boreal spring (MAM(+1)). The early decay of CP warming is also evident in the temporal evolution of SSTA at 160°W (i.e., CP) and the change is significant compared to the inter-model spread (Fig. 10). Note that no significant change is expected in the EP (i.e., 110°W), which is consistent with results from previous studies [e.g., *Cai et al.*, 2014; *Chen et al.*, 2016]. Despite these changes, the two leading modes seem to undergo no fundamental changes between the present and future climates.

Figure 11 displays the changes in fractional variance. There are no significant changes in fractional variance; it increases in 16 models but decreases in 24 models. Interestingly, the inter-model correlation coefficients of variances between the present and future climates are 0.32, which is significant at the 95% confidence level. For the ten best models, the percentage variances explained by EOF1 in the present climate are highly correlated with those in the future climate ($r \sim 0.91$). Another point of note is that in most models, the EOF1 mode of the

historical simulation remains the same as the EOF1 mode of the RCP8.5 simulation, indicating that the transition mode is the most dominant one across all models from the present to future climate. There are only two exceptions. The CMCC-CM3 and CNRM-CM5 predict changes from the present EOF1 (EOF2) into the future EOF2 (EOF1), and vice versa. The cross correlation coefficients between the observed EOF1 (EOF2) and EOF2 (EOF1) in the future climate are very high at 0.83 (0.87) for CMCC-CM3 and 0.80 (0.74) for CNRM-CM5.

The modeled fractional variances of EOF2 also exhibit no significant changes; they increase in 17 models but decrease in 23 models. However, the variance has a tendency to change randomly from the present to the future climate ($r \sim 0.09$), reflecting that future changes in the persistence mode are considerably stochastic and non-directional across all models. Consequently, we speculate that El Niño's transition into La Niña will remain unchanged from the present to future climate, which plays a key role in understanding modeled El Niño diversity. Meanwhile, the persistence of inter-El Niño variability is most sensitive to increasing greenhouse gases. Due to considerable inter-model diversity in the persistence mode, it is extremely difficult to predict the effect of global warming on inter-El Niño variability.

5. Discussion and conclusion

The present study examined the 40 models' reproducibility in relation to the mean spatiotemporal structure and two leading modes of inter-El Niño variability. Compared to the OBS, most of the climate models realistically simulate the spatiotemporal evolution of El Niño and, furthermore, the EOF1 mode, called the "transition mode". However, only two-fifths of the 40 CMIP5 models are successful in reproducing the EOF2 mode that is characterized by spring persistence of El Niño SSTA. There is also considerable inter-model diversity in EOF2 performance, indicating that major model deficiency in simulating inter-El Niño variability is derived from the second EOF mode. Therefore, we selected the ten best models based on the performance of EOF2 using a measurement of PCC and NRMSE.

The future changes from the B10MMM are summarized as follows.

(1) The mean SST evolution shows no robust changes between the present and future climates across all models.

(2) The leading two modes also exhibit no significant changes between the present and future climates, with respect to the spatiotemporal pattern, phase relationship of event-to-event variability, and fractional variance. A small change is only seen in the CP warming of EOF2 that tends to decay earlier in the boreal spring.

(3) While the transition mode is the most dominant mode across all models from the present to future climate, the persistence mode reveals stochastic and non-directional changes

across the models.

Consequently, we argue that the El Niño's transition into La Niña is most important for understanding the modeled inter-El Niño variability and remains unaffected under global warming. The changes in persistence among El Niño events are most susceptible to rising greenhouse gases, thus resulting in high uncertainties in predictions of future changes of inter-El Niño variability.

Note that the future changes in spatial patterns of inter-El Niño variability are somewhat sensitive to the analyzed EOF periods (figure not shown). However, regardless of the EOF time periods, no coherent changes in spatial pattern and fractional variance are revealed from the present climate to the future climate. Our finding of no significant changes in the EP is consistent with results from previous studies [e.g., *Taschetto et al.*, 2014; *Chen et al.*, 2016]. Another point of note is the significant change in the CP of EOF2 during the boreal spring. The SSTA evolution of CM for Niño 4 also reveals a more rapid decay during the following spring under the future climate than for Niño 3 (figure not shown). The earlier decay in the CP may be in part associated with the change in the North Pacific atmospheric circulation. The mid-latitude atmospheric variability during winter is closely related to SST variances in the CP during the following season [*Vimont et al.*, 2003; *Yu et al.*, 2010]. The relevant dynamics are a subject of ongoing study.

There is vigorous debate as to whether greenhouse warming can modulate changes in

ENSO's nonlinearity and asymmetry [e.g., *Yeh and Kirtman*, 2007; *Cai et al.*, 2015]. With this recognition, the changes in inter-La Niña variability should be examined to understand ENSO's nonlinear effect due to changes in the mean state. Substantial issues still remain regarding the realistic simulation of inter-ENSO variability, in spite of great progress made in the ENSO modeling. In particular, effort is needed to improve the ability to simulate the persistence mode and to further understand a diverse continuum of ENSO events. In addition, substantial variations in spatiotemporal evolution will be investigated with respect to various ocean feedbacks (e.g., recharge/discharge oscillator, thermocline, and zonal advection feedbacks) in our future work. Better models and improved understanding of model deficiencies are scientifically important for enabling more reliable projections and predictions under a warmer climate.

Acknowledgments

This study was supported by GRL grant of the National Research Foundation (NRF) funded by the Korean Government (MEST 2011-0021927). K. S. Yun was supported by NRF-2015R1C1A1A01054992. We acknowledge the data providers for producing HadISST1.1 SST data (http://www.metoffice.gov.uk/hadobs/hadisst/) and CMIP5 model output (https://pcmdi.llnl.gov/search/cmip5/).

References

Bellenger, H., E. Guilyardi, J. Leloup, M. Lengaigne, and J. Vialard (2014), ENSO representation in climate models: From CMIP3 to CMIP5, *Climate Dyn.*, *42*, 1999–2018, doi:10.1007/s00382-013-1783-z.

Cai, W., et al. (2014), Increasing frequency of extreme El Niño events due to greenhouse warming, *Nature Climate Change*, *4*, 111-116.

Cai, W., et al. (2015), ENSO and greenhouse warming, *Nature Climate change*, *5*, 849-859.

Capotondi, A., et al. (2015), Understanding ENSO diversity, *Bull. Am. Meteorol. Soc.*, *96*, 921-938, doi:10.1175/BAMS-D-13-00117.1.

Chen, L., T. Li, and Y. Yu (2015), Causes of strengthening and weakening of ENSO amplitude under global warming in four CMIP5 models, *J. Climate*, *28*, 3250-3274.

Chen, W., J.-Y. Lee, K.-J. Ha, K.-S. Yun, and R. Lu (2016), Intensification of the western North Pacific Anticyclone response to the short decaying El Nino event due to greenhouse warming, *J Clim*, Accepted. doi:10.1175/JCLI-D-15-0195.

Collins, M., et al. (2010), The impact of global warming on the tropical Pacific Ocean and El Nino. *Nat. Geosci.*, *3*, 391–397, doi:10.1038/ngeo868.

Ha, K.-J., S.-J. Yoon, K.-Y. Yun, J.-S. Kug, Y.-S. Jang, and J. C. L. Chan (2012), Dependency of typhoon intensity and genesis locations on El Nino phase and SST shift over the western North Pacific, *Theor. Appl. Climatol.*, *109*, 383–395.

Jin, F.-F. (1997), An equatorial ocean recharge paradigm for ENSO. Part I: Conceptual model, *J. Atmos. Sci., 54*, 811-829.

Kao, H. Y., and J. Y. Yu (2009), Contrasting eastern Pacific and central Pacific types of ENSO, *J. Climate, 22*, 615–632, doi:10.1175/2008JCLI2309.1.

Kay, J. E. et al. (2015), The Community Earth System Model (CESM) Large Ensemble Project: A community resource for studying climate change in the presence of internal climate variability, *Bull. Amer. Meteor. Soc., 96*, 1333- 1349.

Kim, K.-M., and K.-M. Lau (2001), Dynamics of monsoon-induced biennial variability in ENSO, *Geophys. Res. Lett., 28*, 315-318.

Kim, S. T., and J.-Y. Yu (2012), The two types of ENSO in CMIP5 models, *Geophys. Res. Lett., 39*, L11704, doi:10.1029/2012GL052006.

Kim, S.-T., et al. (2014), Response of El Nino sea surface temperature variability to greenhouse warming, *Nature Clim. Change*, *4*, 786-790.

Kug, J.-S., F.-F. Jin, and S.-I. An (2009), Two Types of El Niño Events: Cold Tongue El Niño and Warm Pool El Niño, *J. Clim.*, 22, 1499-1515.

Kug, J.-S., and I.-S. Kang (2006), Interactive feedback between ENSO and the Indian Ocean, *J. Clim. 19*, 1784–1801.

Lee, S.-K., P. N. DiNezio, E.-S. Chung, S.-W. Yeh, A. T. Wittenberg, and C. Wang (2014), Spring persistence, transition, and resurgence of El Niño, *Geophys. Res. Lett.*, *41*, doi:10.1002/2014GL062484.

Lopez, H., and B. P. Kirtman (2013), Westerly wind bursts and the diversity of ENSO in CCSM3 and CCSM4, *Geophys. Res. Lett.*, *40*, 4722–4727, doi:10.1002/grl.50913.

McPhaden, M. J., S. E. Zebiak, and M. H. Glantz (2006), ENSO as an integrating concept in Earth science, *Science*, *314*, 1740-1745.

Power, S., F. Delage, C. Chung, G. Kociuba, and K. Keay (2013), Robust twenty-first-century projections of El Nino and related precipitation variability, *Nature*, *502*, 541-545.

Rayner, N. A., et al. (2003), Global analyses of sea surface temperature, sea ice, and night marine air temperature since the late nineteenth century, *J. Geophys. Res.*, *108*, 4407, doi:10.1029/2002JD002670.

Stevenson, S. L. (2012), Significant changes to ENSO strength and impacts in the twenty-first century: Results from CMIP5, *Geophys. Res. Lett.*, *39*, L17703, doi:10.1029/2012GL052759.

Taschetto, A. S., A. S. Gupta, N. C. Jourdain, A. Santoso, C. C. Ummenhofer, and M. H. England. (2014), Cold Tongue and Warm Pool ENSO Events in CMIP5: Mean State and Future Projections, *J. Climate*, *27*, 2861-2885.

Taylor, K. E., R. J. Stouffer, and G. A. Meehl (2012), An overview of CMIP5 and the experiment design. *Bull. Amer. Meteor. Soc*., *93*, 485–498.

Vimont, D. J., J. M. Wallace, and D. S. Battisti (2003), The seasonal footprinting mechanism in the Pacific: Implications for ENSO, *J. Clim.*, *16*, 2668–2675.

Wang, B., R. Wu, and R. Lukas (1999), Roles of the western North Pacific wind variation in thermocline adjustment and ENSO phase transition, *J. Meteor. Soc. Japan.*, 77, 1-16.

Yeh, S.-W., and B. P. Kirtman (2007), ENSO amplitude changes due to climate change projections in different coupled models, *J. Clim.*, *20*, 203- 217.

Yeh, S.-W., J.-S. Kug, and S.-I. An (2014), Recent progress on two types of El Niño: Observations, dynamics, and future changes, *Asia-Pac. J. Atmos. Sci.*, *50*, 69–81.

Yeh, S.-W., J.-S. Kug, B. Dewitte, M.-H. Kwon, B. P. Kirtman, and F.-F. Jin (2009), El Niño in a changing climate, *Nature*, *461*, 511–514.

Yu, J.-Y., H.-Y. Kao, and T. Lee (2010), Subtropics-related interannual sea surface temperature variability in the equatorial central Pacific, *J. Clim.*, *23*, 2869–2884

Yu, J.-Y., H.-Y. Kao, and T. Lee (2010), Subtropics-related interannual sea surface temperature variability in the central equatorial Pacific, J. Clim., 23, 2869–2884.

Yu, J.-Y., Y. Zou, S. T. Kim, and T. Lee (2012), The changing impact of El Niño on US winter temperatures, *Geophys. Res. Lett.*, *39*, L15702, doi:10.1029/2012GL052483.

Yun, K.-S., K.-J. Ha, S.-W. Yeh, B. Wang, and B. Xiang (2015) Critical role of boreal summer North Pacific subtropical highs in ENSO transition, *Climate Dyn.*, *44*, 1979-1992, doi:10.1007/s00382-014-2193-6.

Table 1. Description of CMIP5 models used in the study. "ENS No." indicates the number of ensemble members used in the individual historical and RCP8.5 runs and "El Niño No." is the number of El Niño events identified in each run.

	Model	Institution	Ens No. (HIS-RCP8.5)	El Niño No. (HIS-RCP8.5)
1	**ACCESS1.0**	CSIRO-BOM, Australia	2-1	25-22
2	**ACCESS1.3**	CSIRO-BOM, Australia	3-1	28-23
3	**BCC-CSM1.1**	Beijing Climate Center, China	3-1	30-26
4	**BCC-CSM1.1(m)**	Beijing Climate Center, China	3-1	33-30
5	**BNU-ESM**	College of Global Change and Earth System Science, China	1-1	32-23
6	**CanESM2**	Canadian Centre for Climate Modelling and Analysis, Canada	5-5	28-26
7	**CCSM4**	National Center for Atmospheric Research, USA	6-6	24-26
8	**CESM1(BGC)**	Community Earth System Model Contributions, USA	1-1	25-26
9	**CESM1(CAM5)**	Community Earth System Model Contributions, USA	3-3	24-29

10	**CESM1(CAM5.1,FV2)**	Community Earth System Model Co ntributions, USA	4-1	29-27
11	**CESM1(WACCM)**	Community Earth System Model Co ntributions, USA	1-3	25-27
12	**CMCC-CM**	Centro Euro-Mediterraneo per I Cambiamenti Climatici, Italy	1-1	27-24
13	**CMCC-CMS**	Centro Euro-Mediterraneo per I Cambiamenti Climatici, Italy	1-1	30-27
14	**CNRM-CM5**	Centro Euro-Mediterraneo per I Cambiamenti Climatici, Italy	10-5	33-21
15	**CSIRO-Mk3.6.0**	CSIRO-QCCCE, Australia	10-10	22-21
16	**EC-EARTH**	EC-EARTH consortium, Various	2-1	28-24
17	**FGOALS-g2**	LASG-CESS, China	5-1	30-27
18	**FIO-ESM**	First Institute of Oceanography, SO A, China	3-2	31-37
19	**GFDL-CM3**	NOAA Geophysical Fluid Dynamics Laboratory, USA	5-1	33-30
20	**GFDL-ESM2G**	NOAA Geophysical Fluid Dynamics Laboratory, USA	1-1	30-22

21	**GFDL-ESM2M**	NOAA Geophysical Fluid Dynamics Laboratory, USA	1-1	24-26
22	**GISS-E2-H**	NASA Goddard Institute for Space Studies, USA	6-2	26-28
23	**GISS-E2-H-CC**	NASA Goddard Institute for Space Studies, USA	1-1	35-31
24	**GISS-E2-R**	NASA Goddard Institute for Space Studies, USA	6-2	30-28
25	**GISS-E2-R-CC**	NASA Goddard Institute for Space Studies, USA	1-1	29-28
26	**HadGEM2-AO**	Met Office Hadley Centre, UK	1-1	24-19
27	**HadGEM2-CC**	Met Office Hadley Centre, UK	1-3	28-23
28	**HadGEM2-ES**	Met Office Hadley Centre, UK	5-4	24-21
29	**INM-CM4**	Institute for Numerical Mathematics, Russia	1-1	24-17
30	**IPSL-CM5A-LR**	Institut Pierre-Simon Laplace, France	6-4	27-25
31	**IPSL-CM5A-MR**	Institut Pierre-Simon Laplace, France	3-1	25-24
32	**IPSL-CM5B-LR**	Institut Pierre-Simon Laplace, France	1-1	28-26
33	**MIROC5**	MIROC, Japan	5-3	25-26

34	**MIROC-ESM**	MIROC, Japan	3-1	24-23
35	**MIROC-ESM-CHEM**	MIROC, Japan	1-1	24-22
36	**MPI-ESM-LR**	Max-Planck-Institut für Meteorologie, Germany	3-3	27-25
37	**MPI-ESM-MR**	Max-Planck-Institut für Meteorologie, Germany	3-1	23-20
38	**MRI-CGCM3**	Meteorological Research Institute, Japan	5-1	28-19
39	**NorESM1-M**	Norwegian Climate Centre, Norway	3-1	28-22
40	**NorESM1-ME**	Norwegian Climate Centre, Norway	1-1	31-23

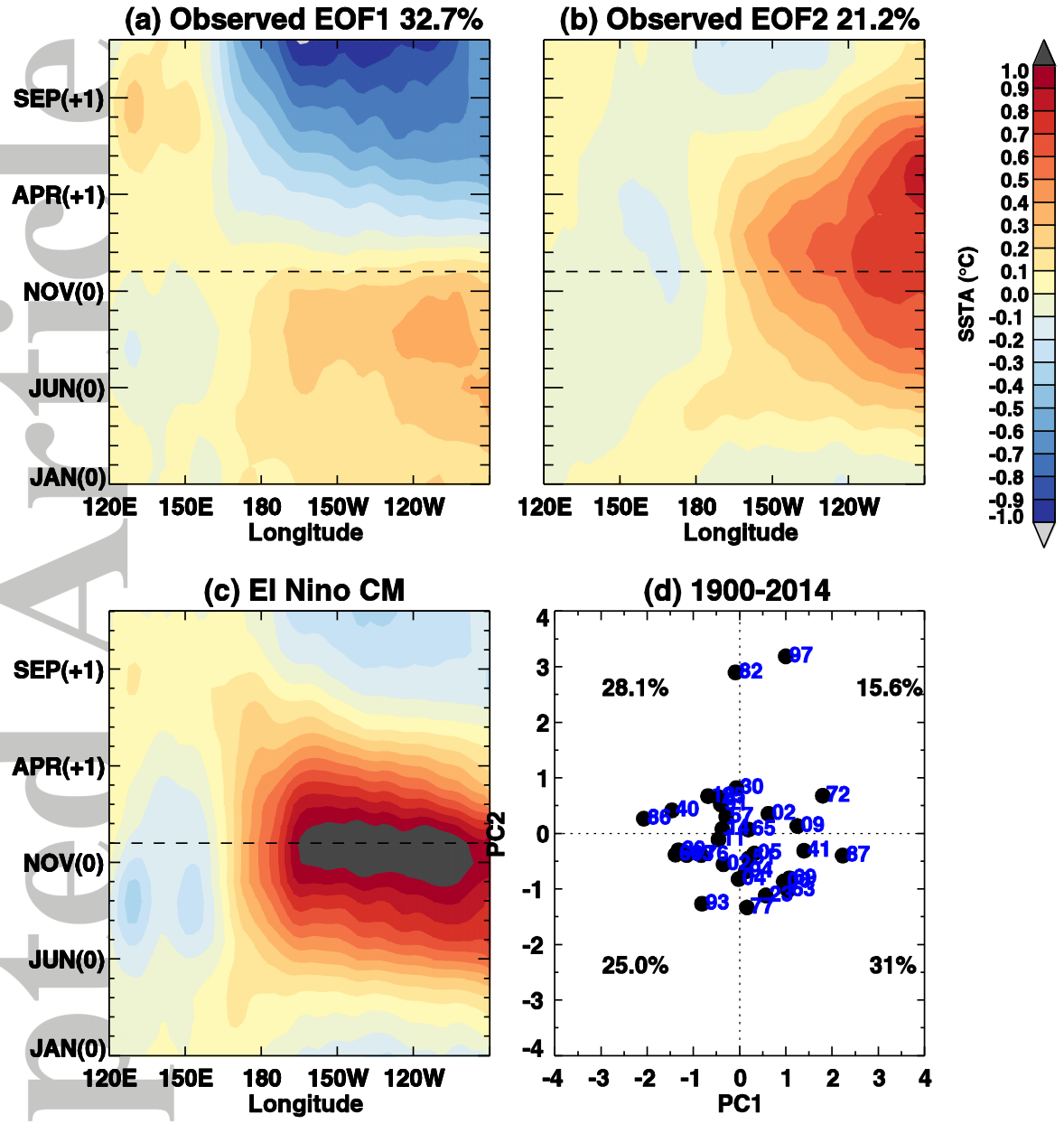

Figure 1. (a, b) Time-longitude plots of the first two inter-event EOFs of tropical SSTAs averaged over 5°S-5°N for 32 El Niño events. (c) Composite mean (CM) of SSTAs for El Niño events. (d) Scatter plot of normalized PC1 versus PC2. The HadISST data is used for the observation (OBS).

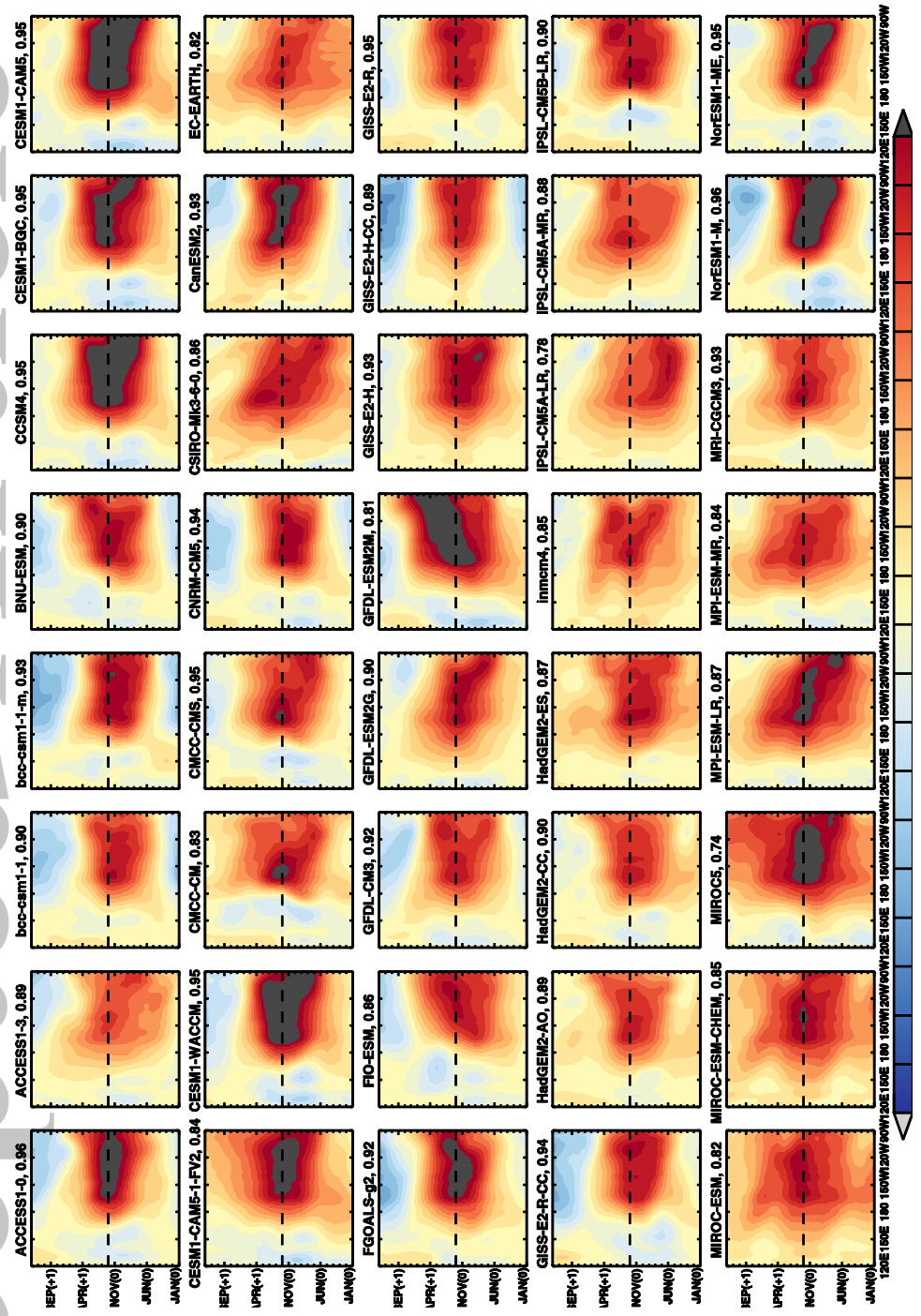

Figure 2. Longitude-time plot of El Niño SSTA CMs obtained from the historical run of 40 CMIP5 models during 1900-2005.

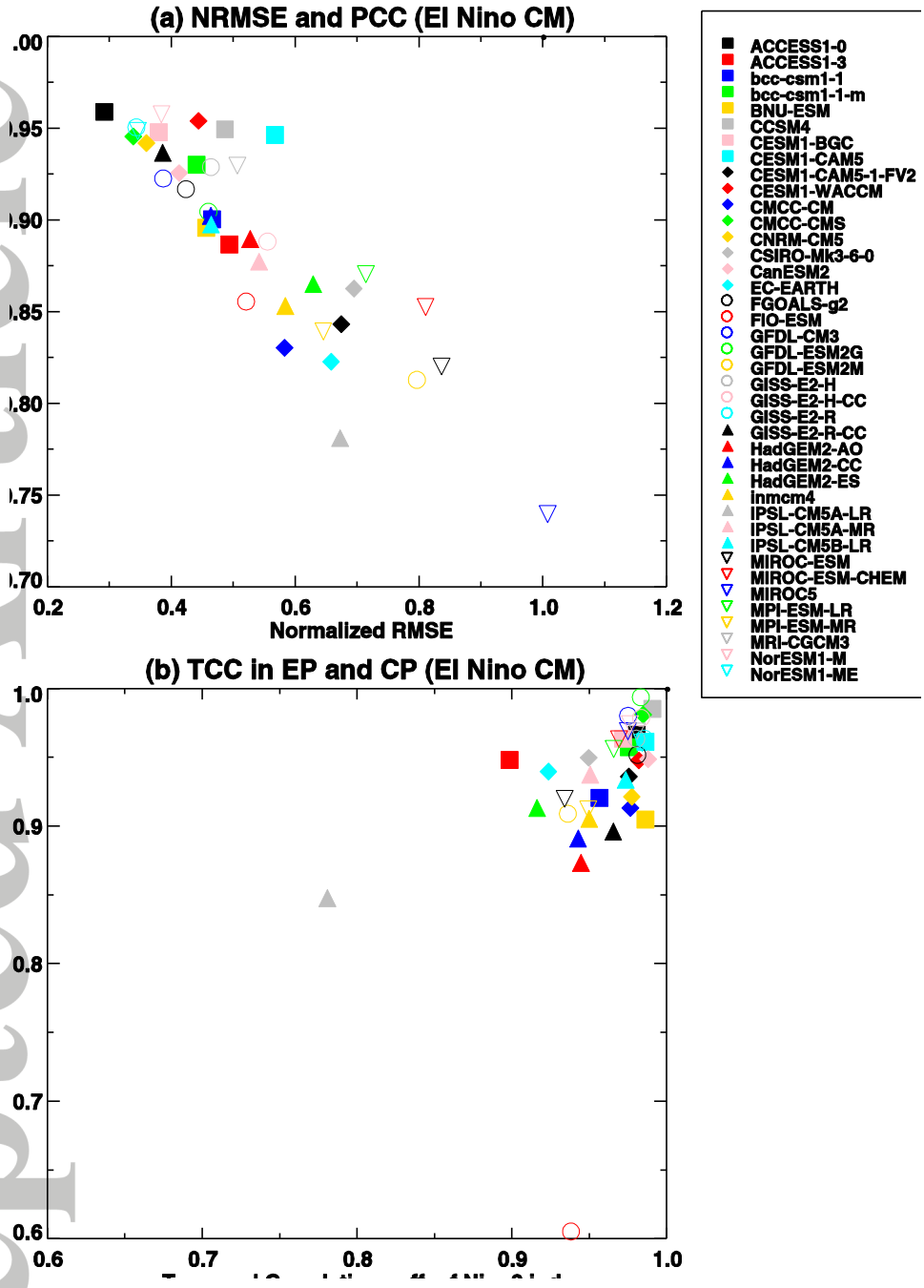

Figure 3. (a) Scatter plot of NRMSE (x-axis) and pattern correlation coefficients (y-axis) between OBS and individual CMIP5 models for the El Niño CMs in the historical run. Here, NRMSE is domain-averaged RMSE normalized by the observed standard deviation. (b) Scatter plot of temporal correlation coefficients between OBS and individual CMIP5 models for the Niño 3 and Niño 4 SSTA CMs.

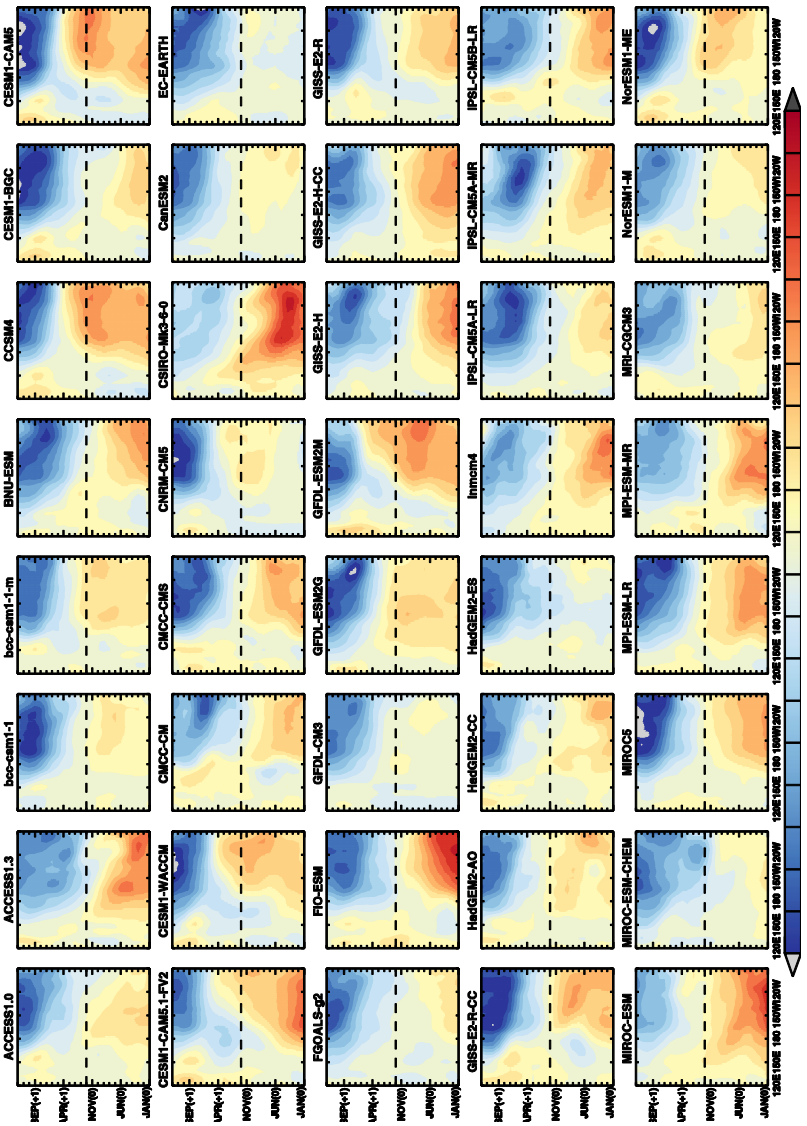

Figure 4. Longitude-time plots of the first EOF (EOF1) for inter-El Niño variability obtained from the historical run of 40 CMIP5 models during 1900-2005.

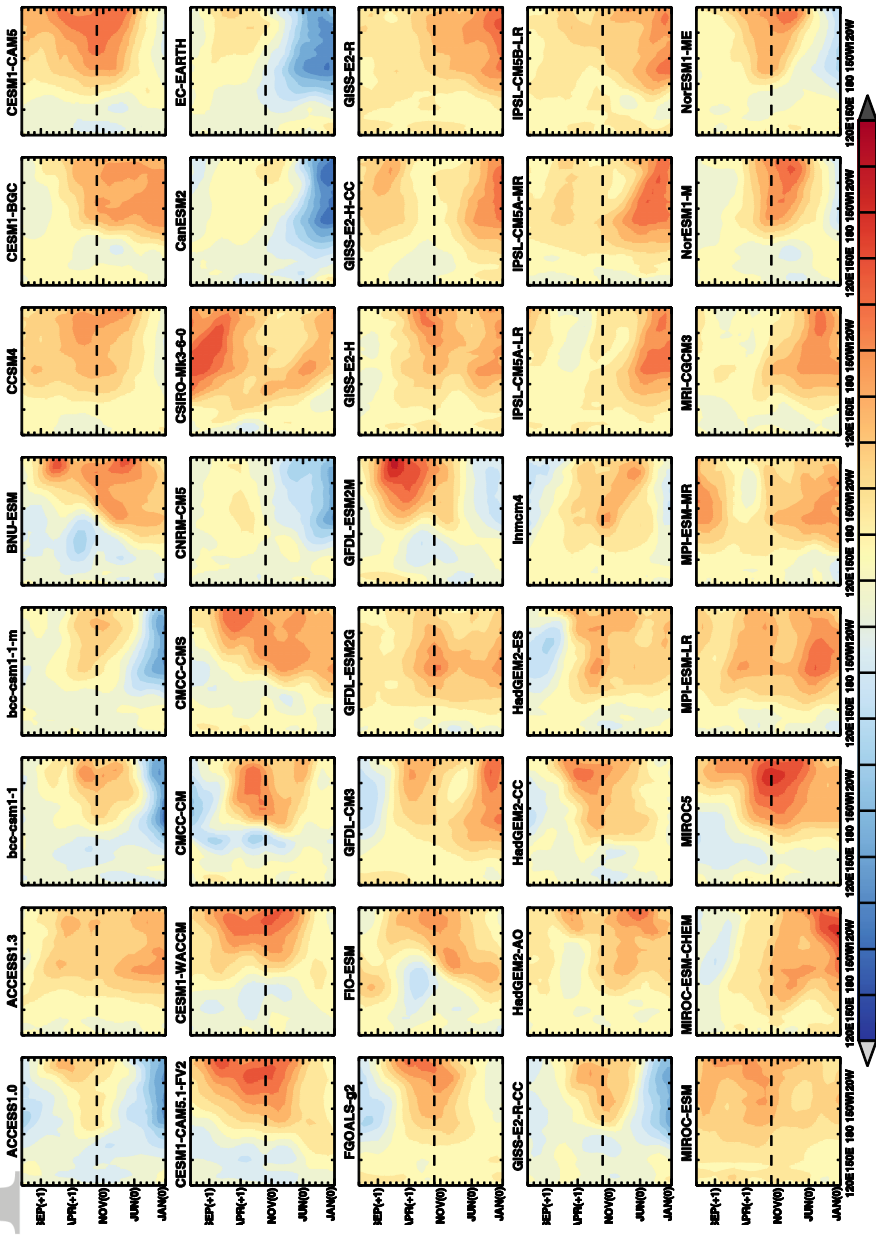

Figure 5. Same as Fig. 4, but for the second EOF (EOF2).

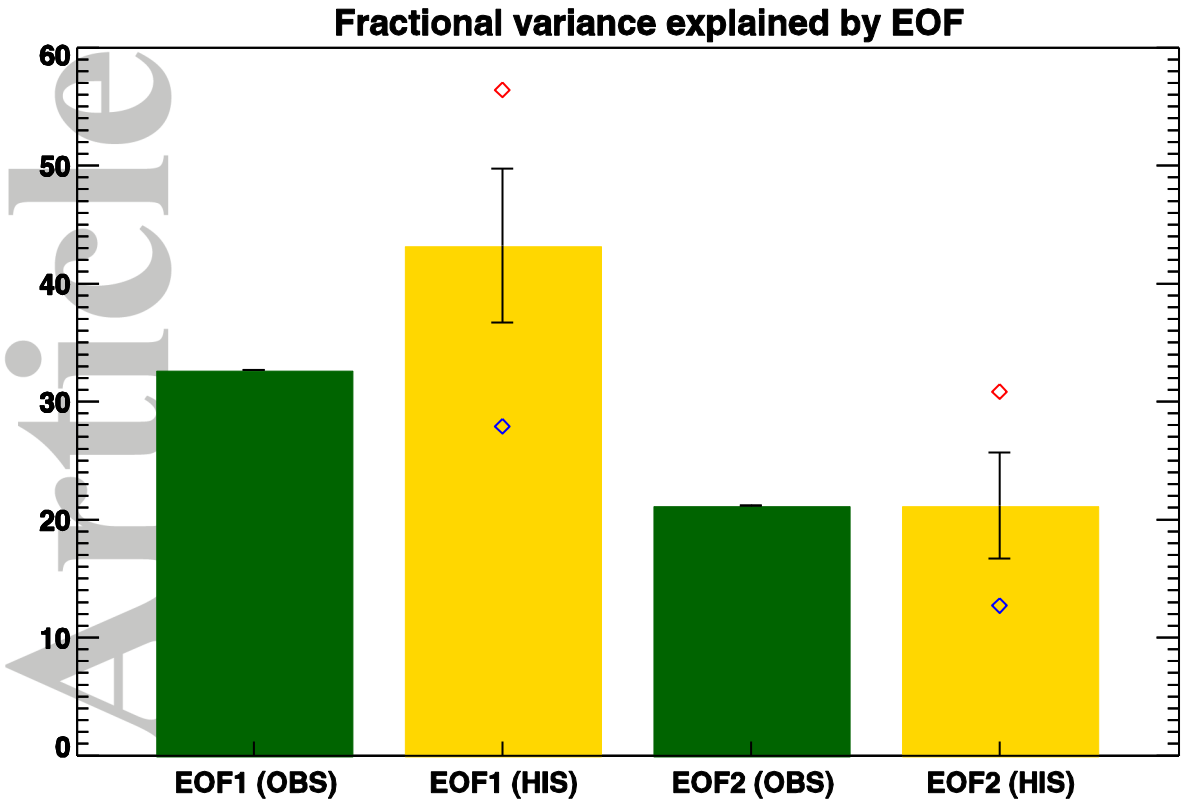

Figure 6. Fractional variance explained by the first two leading modes (EOF1 and EOF2) in the OBS (green) and by the multi-model mean of historical simulations (yellow). The vertical error bar in yellow indicates one standard deviation of inter-model variability. Blue and red diamonds denote the minimum and maximum of fractional variances in CMIP5 models, respectively.

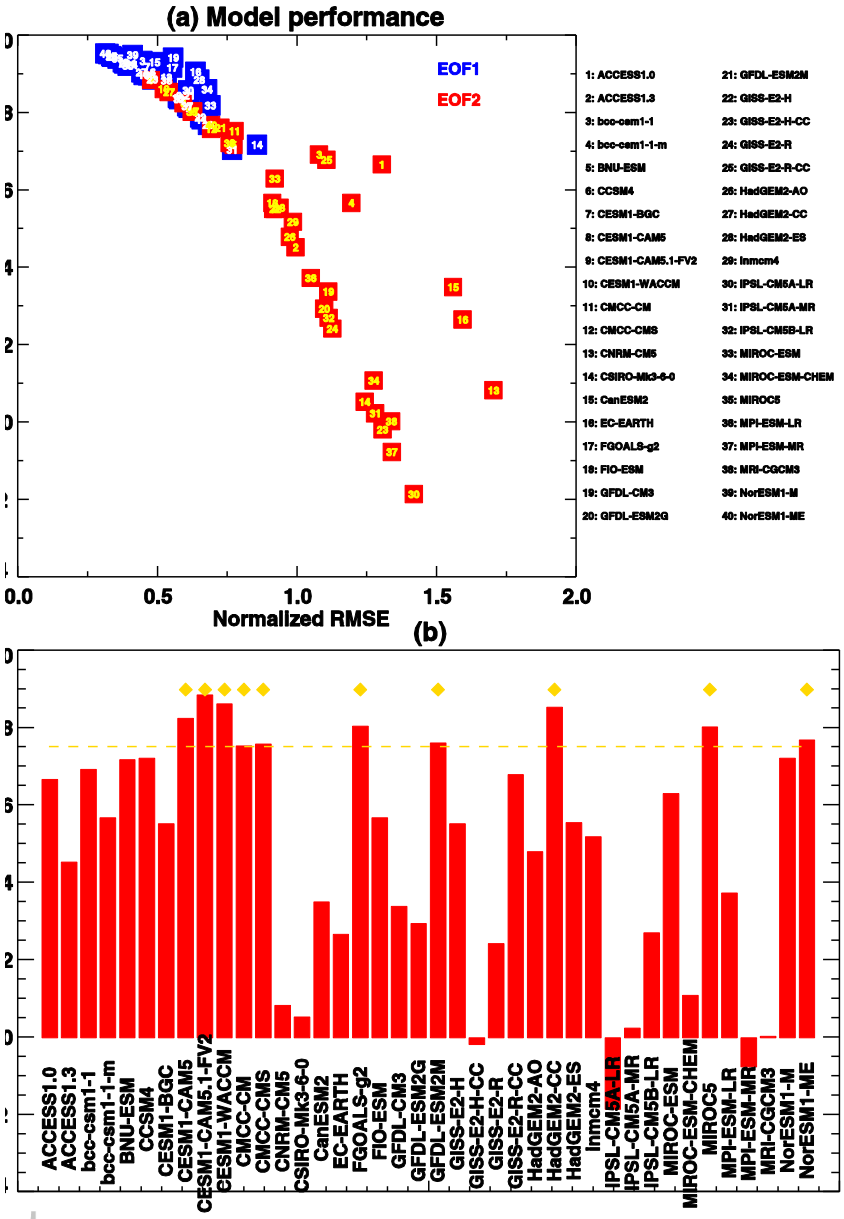

Figure 7. (a) Scatter plot of NRMSE (x-axis) and pattern correlation coefficients (y-axis) between OBS and individual CMIP5 models for the first two EOFs in the historical run. (b) Bar plot of correlation coefficients between OBS and CMIP5 models for EOF2. Diamonds above the bar indicate the ten best models with respect to performance in simulating EOF2.

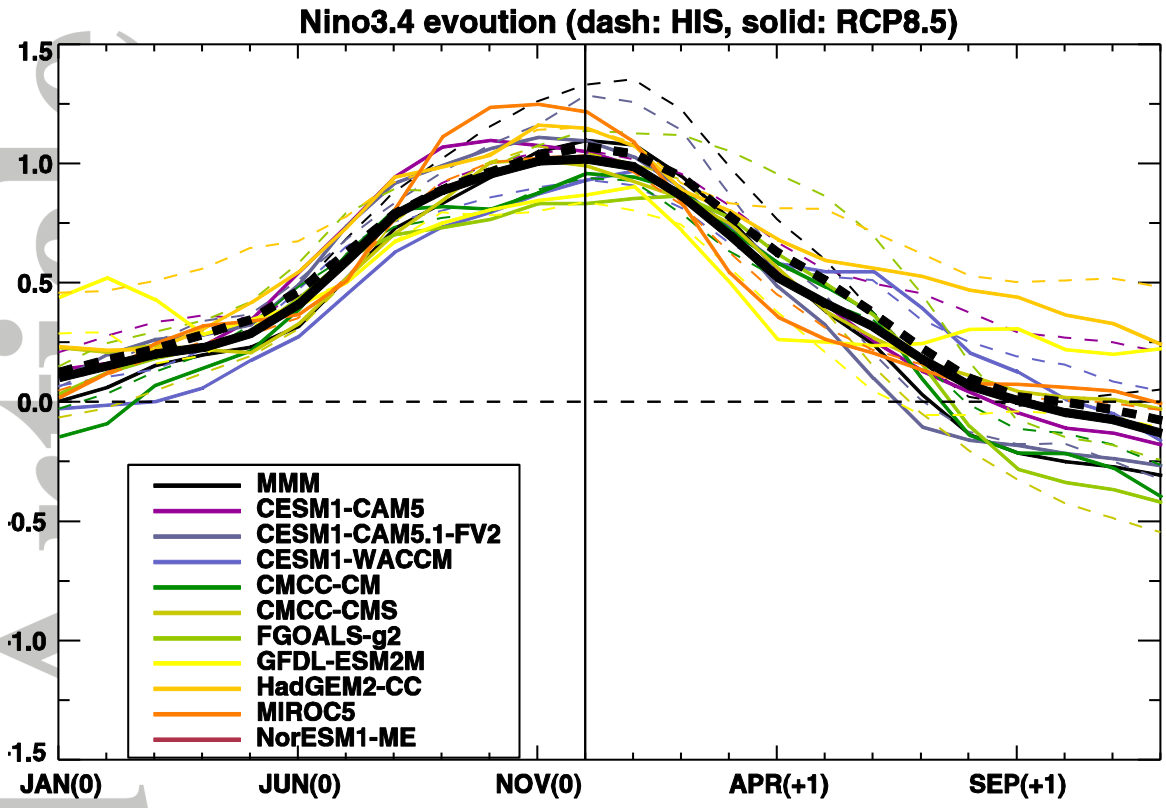

Figure 8. Temporal evolution of Niño 3.4 SSTA CMs for the ten best CMIP5 models in the historical (dashed lines) and RCP8.5 (solid lines) runs. Thick black lines indicate the multi-model mean for the ten best models (i.e., B10MMM).

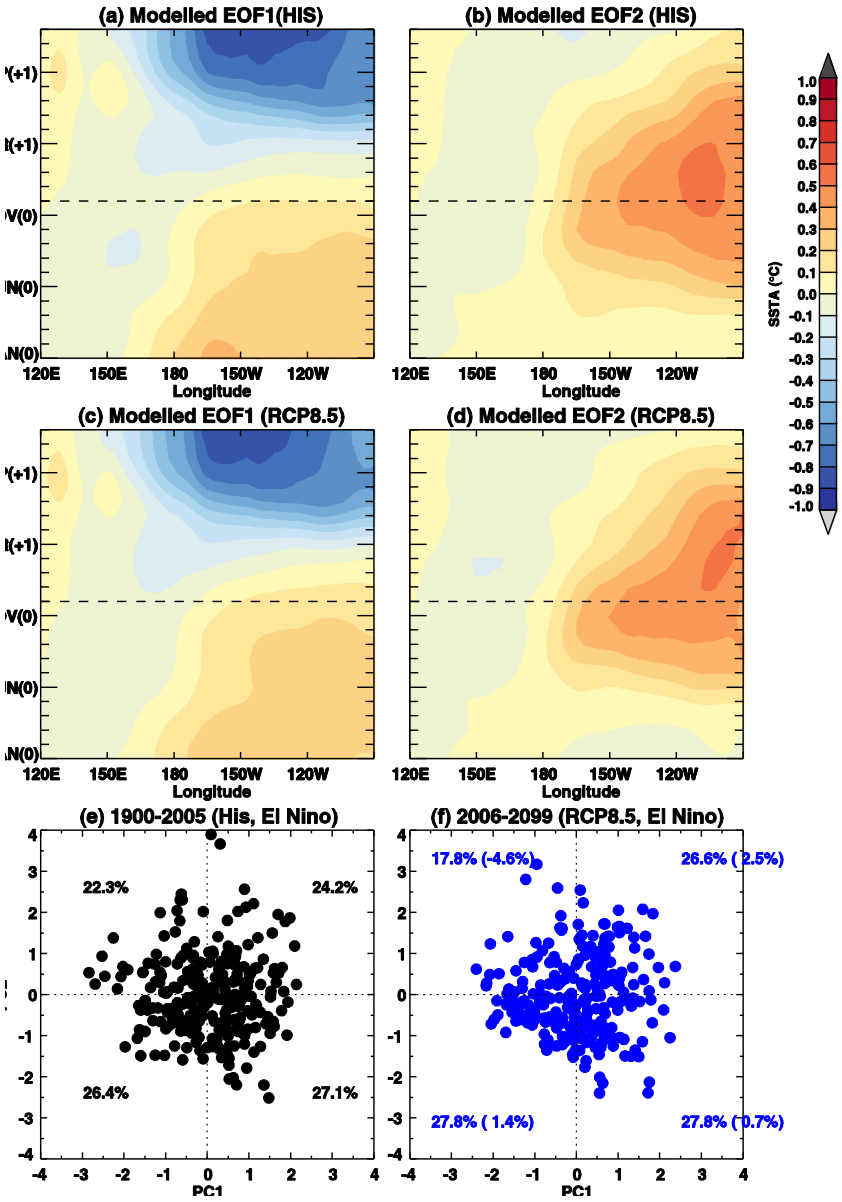

Figure 9. (a) Longitude-time plot of B10MMM for the first two modeled EOFs of tropical SSTAs averaged over 5°S-5°N for El Niño variability in the historical run. (b) Same as (a), but for the RCP8.5 run. (c) Scatter plots of normalized time series of PC1 versus PC2 in the historical (left) and RCP8.5 (right) runs.

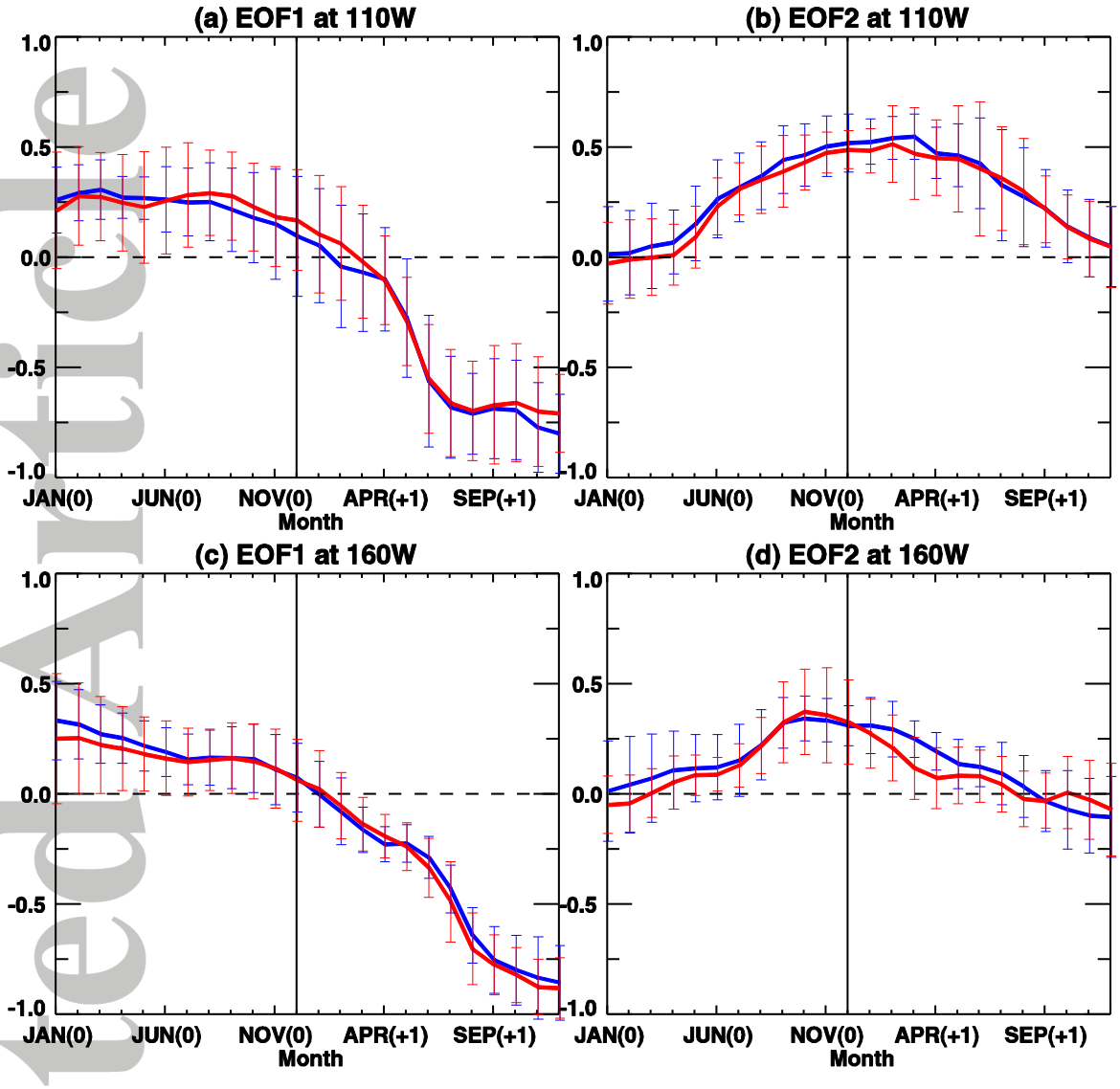

Figure 10. (a, b) Temporal SSTA evolution of B10MMM for (a) EOF1 and (b) EOF2 at 110°W longitude in the historical (blue) and RCP8.5 (red) runs. (c, d) Same as (a, b), but for at 160°W longitude. The vertical bar indicates one standard deviation among the ten best models.

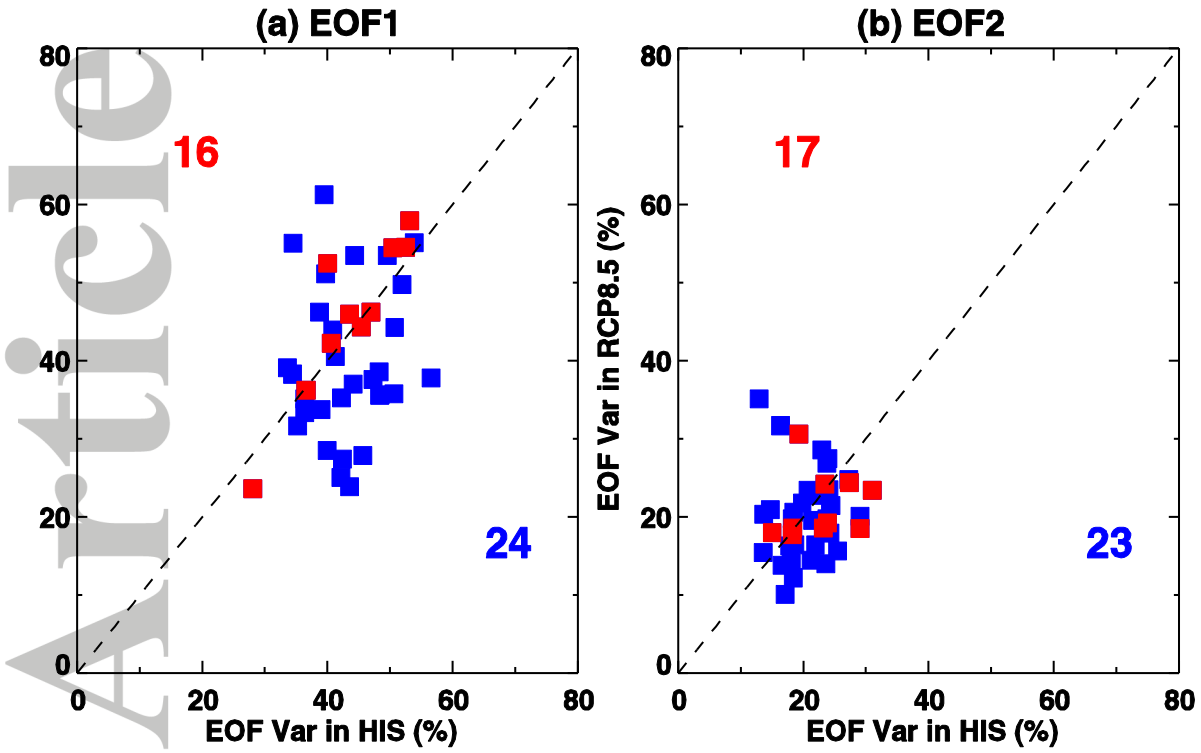

Figure 11. Fractional variance explained by (a) EOF1 and (b) EOF2 in the historical (x-axis) and RCP8.5 (y-axis) runs. Red boxes indicate the ten best models shown in Fig. 7.